New Method for Extracting Neutron Structure Functions from Nuclear Data

Yonatan Kahn

Northwestern University, Evanston, Illinois 60208, USA, and

Jefferson Lab, Newport News, Virginia 23606, USA

W. Melnitchouk

Jefferson Lab, Newport News, Virginia 23606, USA

S. A. Kulagin

Institute for Nuclear Research,

Moscow 117312, Russia

Abstract

We propose a new method for extracting neutron structure functions from inclusive structure functions of nuclei, which employs an iterative procedure of solving integral convolution equations. Unlike earlier approaches, the new method is applicable to both spin-averaged and spin-dependent structure functions. We test the reliability of the method on unpolarized F_2 and polarized g_1 structure functions of the deuteron in both the nucleon resonance and deep inelastic regions. The new method is able to reproduce known input functions of almost arbitrary shape to very good accuracy with only several iterations.

I. INTRODUCTION

Understanding the detailed structure of the nucleon remains one of the central problems of the strong nuclear interactions. This is particularly challenging in the so-called transition region at momentum scales ~ 1 GeV, where neither perturbative Quantum Chromodynamics (QCD) nor effective hadronic theories provide adequate descriptions of physical observables.

Over the past few years one of the fascinating developments in the study of this transition has been the phenomenon of quark-hadron duality in inclusive electron–nucleon (and nucleus) scattering. Here the structure functions in the region dominated by low-lying resonant excitations of the nucleon are found to closely resemble, on average, the deep inelastic structure functions describing the high-energy cross section [1]. Since QCD at high energy and momentum transfers can be treated perturbatively, but is highly nonperturbative at low energies where hadronic degrees of freedom are prominent, this duality provides an intimate link between the two regimes.

Recent experiments have sought to quantify quark-hadron duality by determining its flavor, spin, and nuclear dependence, while theoretical endeavors have attempted to understand its dynamical origin from a more fundamental basis (for a review see Ref. [2]). In particular, even from simple quark model arguments one expects intriguingly different behaviors of duality for the proton and for the neutron [3].

While duality for the proton has been tested to rather good accuracy in recent measurements, for both unpolarized and polarized scattering [4, 5], there is almost a complete absence of analogous empirical information on the neutron. This lack of knowledge has prevented the various theoretical models from being adequately tested, and has impeded progress in unraveling the microscopic origin of the duality phenomenon. The difficulty with obtaining data on neutron structure functions is of course the absence of free neutron targets. As a result one often makes use of light nuclei such as deuterium [6] or ^{3}He [7] as effective neutron targets, assuming that the nuclear corrections are negligible.

Even when nuclear effects are considered, there exist practical difficulties with extracting information on the neutron from nuclear data. Some attempts have been made to obtain the spin-averaged F_2^n structure function from proton and deuterium data in the deep inelastic scattering region, where the exchanged four-momentum transfer squared Q^2 is large (~ 5 GeV^2 or greater). A common approach has made use of the so-called smearing factor

method [8], where after an initial guess for F_2^n one iterates the solution in order to eliminate the dependence of the extracted neutron structure function on the starting point.

In practice the smearing factor method has only been applied to the unpolarized F_2 structure function and only in deep inelastic kinematics [9]. The robustness of this procedure is guaranteed only for functions which do not change sign, and for spin-dependent structure functions, which can have several zeros, the usual prescription is inadequate. Furthermore, in the nucleon resonance region, where there exists non-trivial resonant structure, it is not *a priori* clear whether it is even possible to extract resonance structure that has been smeared out by nucleon Fermi motion.

In this paper we propose a new method in which the nuclear effects are parameterized via an additive correction to the free nucleon structure functions. In contrast to the more common multiplicative method, which is problematic for structure functions with zeros, the new method can be used for functions of almost arbitrary shape, which allows access to neutron structure in both the deep inelastic and resonance regions. By iterating the solution, the dependence on the initial guess for the neutron structure function is eliminated, and in practice a reliable extraction can be achieved after only several iterations.

In Sec. II we present the formalism for computing nuclear structure functions at finite Q^2 within the nuclear impulse approximation. While the formalism is general and can be applied to any nucleus, to illustrate the features of the new extraction method we focus on the specific case of the deuteron. In Sec. III we present the details of the new method, and discuss other methods which have been used to extract neutron structure functions from nuclear data, including the smearing factor method, and a direct method of inverting integral equations which has previously been used in Refs. [10, 11]. Our results are presented in Sec. IV for spin-averaged and spin-dependent structure functions, in both the resonance and deep inelastic regions. Using known input functions constructed from resonance and leading twist structure function parameterizations, we demonstrate the accuracy of the extraction method and provide a detailed discussion of its convergence to the exact results as a function of the number of iterations and the first guess in the iteration. Finally, in Sec. V we summarize our results and preview future applications of the new method.

II. NUCLEAR STRUCTURE FUNCTIONS

The usual framework for computing structure functions of nuclei at large x is the relativistic nuclear impulse approximation, in which the lepton probe scatters from the nucleus incoherently via the scattering from its bound proton and neutron constituents. In this approximation the nuclear structure functions can be written as convolutions of the bound nucleon structure functions and nucleon light-cone momentum distributions in the nucleus [12, 13, 14, 15, 16, 17, 18, 19].

In particular, for the spin-averaged F_2 structure function of a nucleus A we have:

$$F_2^A(x, Q^2) = \left(f_0^{p/A} \otimes F_2^p \right)(x, Q^2) + \left(f_0^{n/A} \otimes F_2^n \right)(x, Q^2) , \qquad (1)$$

where $x = Q^2/2M_A\nu$ is the Bjorken scaling variable (per nucleon), M_A is the nuclear mass and ν is the energy transfer, and the symbol $\otimes$ denotes the convolution

$$\left(f_0^{N/A} \otimes F_2^N \right)(x, Q^2) \equiv \int_x^{M_A/M} dy \, f_0^{N/A}(y, \gamma) \, F_2^N\left(\frac{x}{y}, Q^2\right) , \qquad (2)$$

with M the nucleon mass. The function $f_0^{N/A}$ is the light-cone momentum distribution of nucleons N in the nucleus, and is a function of the light-cone momentum fraction y of the nucleus carried by protons ($N = p$) or neutrons ($N = n$), and of the virtual photon "velocity" γ in the target rest frame, $\gamma = |\boldsymbol{q}|/q_0 = (1 + 4M^2x^2/Q^2)^{1/2}$. For moderate Q^2 values $Q^2 \sim 1 - 10$ GeV^2, γ ranges between unity and ≈ 2. As discussed in Ref. [18, 19], taking the full Q^2 dependence of the smearing function into account is vital for discussing nuclear structure functions at large-x or resonance kinematics.

For the spin-dependent nuclear g_1^A and g_2^A structure functions, one has a set of coupled equations involving both the nucleon g_1^N and g_2^N structure functions [18],

$$xg_i^A(x, Q^2) = \left(f_{ij}^{p/A} \otimes xg_j^p \right)(x, Q^2) + \left(f_{ij}^{n/A} \otimes xg_j^n \right)(x, Q^2) , \quad i, j = 1, 2 \qquad (3)$$

where $f_{ij}^{N/A}$ are the spin-dependent nucleon light-cone momentum distribution functions in the nucleus, and a sum over repeated indices j is implied. In contrast to F_2^A, which receives contributions only from the nucleon F_2^N structure function, the spin-dependent structure functions at finite Q^2 involve also non-diagonal contributions $f_{12}^{N/A}$ and $f_{21}^{N/A}$. (Note that both the transverse F_T^A and longitudinal F_L^A structure functions individually receive non-diagonal contributions, whereas F_2^A does not [16].) In the Bjorken limit, the distribution

4

$f_{12}^{N/A}$ vanishes, and the expression for the g_1 structure function becomes diagonal. Equations (1) and (3) can be viewed as equations in the single independent variable x for fixed values of Q^2. In the following, for ease of notation we suppress the dependence of the structure functions on Q^2.

The light-cone momentum distribution functions in Eqs. (1) and (3) (also referred to as *smearing functions*) can in general be calculated from nuclear spectral functions which account for the ground state wave function of the nucleus and the excitation spectrum of the spectator nuclear system, including the continuum spectrum. Since the characteristic energies and momenta of the bound nucleons are small compared with the nucleon mass M, the unpolarized distribution f_0 and the spin-dependent diagonal distributions f_{11} and f_{22} are sharply peaked about $y = 1$.

In this analysis we will focus on the case of the deuteron, for which the smearing functions have recently been evaluated in the weak binding approximation [16, 18], including the finite-Q^2 corrections encoded through the dependence on γ. Note that in the isospin symmetric limit the proton and neutron distributions in the deuteron are identical, $f^{p/d} = f^{n/d} \equiv f$, and we shall in the following omit the superscripts on these distributions.

The unpolarized f_0 distribution function is given in terms of the deuteron wave function $\psi_d(p)$ by [16, 17]

$$f_0(y, \gamma) = \int \frac{d^3p}{(2\pi)^3} |\psi_d(p)|^2 \left(1 + \frac{\gamma p_z}{M}\right) \frac{1}{\gamma^2} \left[1 + \frac{(\gamma^2 - 1)}{y^2} \left(1 + \frac{2\varepsilon}{M} + \frac{p^2}{2M^2}(1 - 3\hat{p}_z^2)\right)\right]$$
$$\times \delta\left(y - 1 - \frac{\varepsilon + \gamma p_z}{M}\right) , \tag{4}$$

where $\varepsilon = \varepsilon_d - p^2/(2M)$, with $\varepsilon_d = -2.2$ MeV the deuteron binding energy. The analogous spin-dependent light-cone distributions f_{ij} are given explicitly in Ref. [18]. For $\gamma = 1$ the f_0 distribution is normalized to the number of protons or neutrons in the deuteron, while f_{11} is normalized to the nucleon polarization in the deuteron,

$$\int_0^{M_A/M} dy \, f_0(y, 1) = 1 , \tag{5}$$

$$\int_0^{M_A/M} dy \, f_{11}(y, 1) = 1 - \frac{3}{2} \, \omega_d , \tag{6}$$

where ω_d is the deuteron D-state probability. For the Paris deuteron wave function [20] used here $\omega_d = 5.8\%$. At finite Q^2, or $\gamma > 1$, these normalization conditions are no longer satisfied, and the distributions do not have probabilistic interpretations.
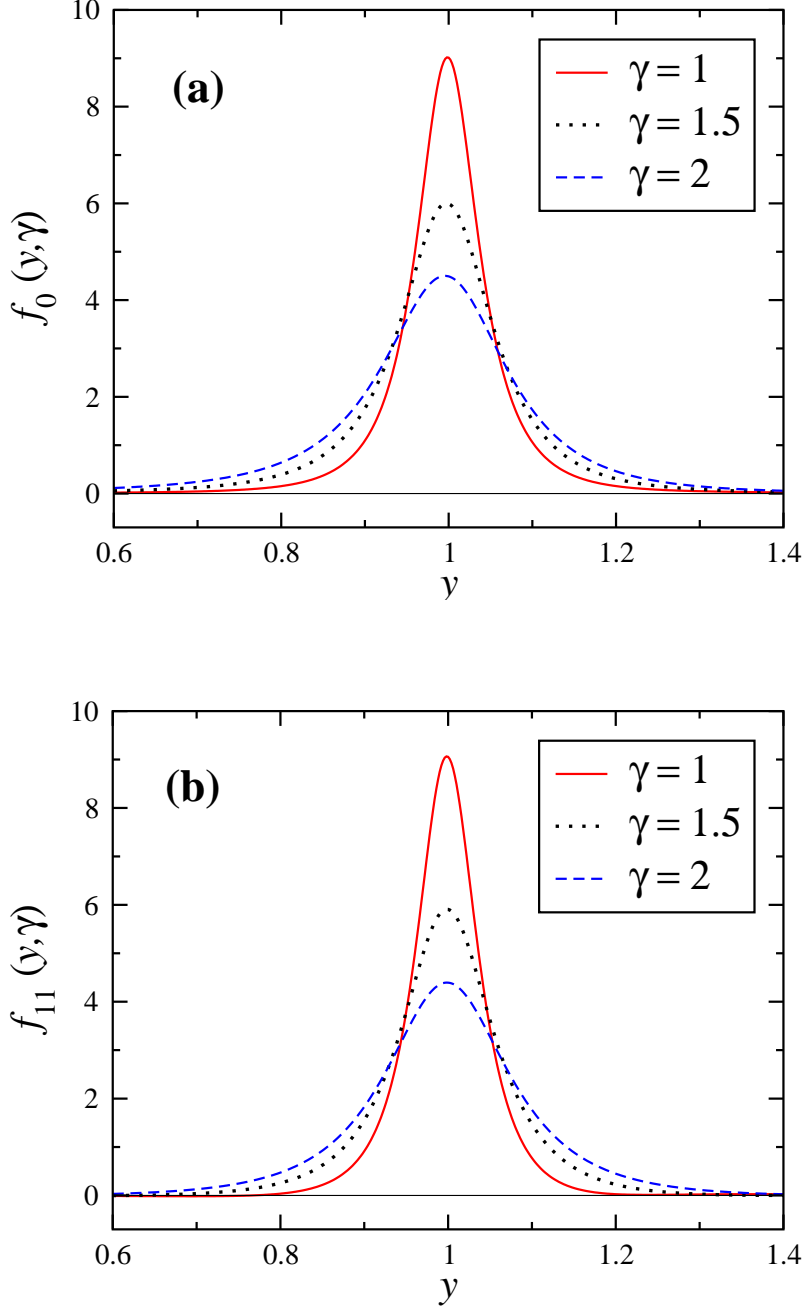
5

FIG. 1: (Color online) Nucleon distribution functions in the deuteron for $\gamma = 1$ (solid), 1.5 (dotted) and 2 (dashed): (a) $f_0(y, \gamma)$ distribution for the F_2^d structure function, (b) $f_{11}(y, \gamma)$ distribution for the xg_1^d structure function.

In Fig. 1 we show the $f_0(y, \gamma)$ distribution for the unpolarized F_2^d structure function [16] and the diagonal $f_{11}(y, \gamma)$ distribution for the polarized xg_1^d structure function [18], for $\gamma = 1$, 1.5 and 2, using the deuteron wave function obtained from the Paris nucleon–nucleon

potential [20]. For $\gamma = 1$ the (Q^2-independent) distributions are peaked sharply around $y = 1$, and decrease rapidly with increasing $|y - 1|$, so that by $|y - 1| > 0.4$ they become almost negligible. For larger γ the distributions become broader, with a larger width and smaller height at the peak. For $\gamma = 2$ the height of the peak is approximately half of that for $\gamma = 1$.

The shapes of the unpolarized and polarized distributions are very similar, with $\approx 0.5\%$ differences between f_0 and f_{11} at the peak for $\gamma = 1$, and $\lesssim 2.5\%$ for $\gamma = 2$. While the spin-averaged function f_0 is constrained to be positive, the spin-dependent f_{11} function, which involves a difference of distributions of nucleons with spins aligned and anti-aligned with that of the deuteron, need not be positive. For values of $y < 0.8$ the $f_{11}(y, \gamma = 1)$ distribution in fact becomes slightly negative, as is (barely) visible in Fig. 1, although the smearing functions here are close to zero.

Before proceeding to the discussion of extraction methods using these distributions, we should note that while the impulse approximation (scattering from individual nucleons in the nucleus) provides the main contribution to nuclear deep inelastic scattering, in realistic calculations of nuclear structure functions other effects are also known to play a role. These include nuclear shadowing and meson exchange currents at small x, final state interactions of the produced hadronic state, relativistic effects, and off-shell corrections to the bound nucleon structure functions [16]. Some of these may be formulated within generalized convolutions, either as two-dimensional convolutions with off-shell structure functions [12, 13, 15], or in terms of exchanged-meson smearing functions [21], and the techniques discussed here may be applicable. Others, such as relativistic corrections, go beyond the convolution approximation [12], and must be included as additive corrections to the convolution. Explicit calculations of final state interactions in the quasi-elastic region have suggested that rescattering effects decrease with increasing Q^2 [22], and in addition partly cancel in inclusive inelastic cross sections when summed over several exclusive channels [23].

In the present analysis we do not attempt to provide a complete description of nuclear structure functions; instead we wish to study the usefulness of the new method of unsmearing nucleon structure functions within the conventional convolution framework. Once we establish the methodology of the new method, additional effects beyond the convolution approximation can be considered in actual data analyses.

III. EXTRACTION METHODS

Having outlined the formalism for computing structure functions of nuclei in terms of those of nucleons, in this section we review several methods for extracting neutron structure functions from nuclear (in practice, deuterium) data, including the new "additive" method proposed in this paper. To extract the neutron structure function from proton and nuclear data at a given Q^2, one first convolutes (or *smears*) the proton structure function $\mathcal{F}^p$, where $\mathcal{F} = F_2$ or $xg_{1,2}$, with the appropriate smearing function,

$$\widetilde{\mathcal{F}}^p(x) \equiv (f \otimes \mathcal{F}^p)(x) , \tag{7}$$

where $f = f_0$ for the unpolarized F_2 structure function, and $f = f_{ij}$ for the polarized $g_{1,2}$ structure functions. Subtracting the smeared proton $\widetilde{\mathcal{F}}^p$ from the nuclear structure function, one obtains an effective smeared neutron structure function

$$\widetilde{\mathcal{F}}^n(x) = \mathcal{F}^d(x) - \widetilde{\mathcal{F}}^p(x) , \tag{8}$$

and then solves the equation

$$\widetilde{\mathcal{F}}^n(x) = (f \otimes \mathcal{F}^n)(x) \tag{9}$$

for $\mathcal{F}^n(x)$. Note that for a fixed Q^2, γ is a function of x alone, so in practice the smearing functions acquire an x dependence.

A. Direct solution

Equation (9) is a system of so-called Volterra integral equations of the first kind, which take the general form

$$g(x) = \int_x^{y_{\max}} dy \; K(x,y) \, z(y) , \tag{10}$$

where $g(x)$ and $K(x,y)$ (the kernel) are known functions and z is unknown. The general theory of Volterra equations is quite extensive, see for example Ref. [24]. Most Volterra equations have no closed-form solution, but numerical solutions for first-kind equations are quite simple. Dividing the interval $0 < y < y_{\max}$ into a grid of width h by $y_a = ah$, with $a = 0, 1, \ldots, N$, and using a quadrature method such as the trapezoidal rule or Simpson's rule, one can approximate the integral in Eq. (10) by a discrete sum

$$g_a = \sum_{b=a}^{N} K_{ab} \, z_b , \tag{11}$$

8

reducing the numerical solution to a problem of matrix inversion: $\mathbf{z} = \mathbf{K}^{-1}\mathbf{g}$. In fact, because of the variable lower limit of integration $y = x$, the matrix $\mathbf{K}$ is upper-triangular, and the inversion is almost trivial. This method has been utilized in Refs. [10, 11] in a similar application. The method fails, though, if $\mathbf{K}$ is singular.

Letting $t = x/y$ and $v = x/y_{max}$, Eq. (9) can be expressed in the form of Eq. (10):

$$\widetilde{\mathcal{F}}^n(y_{max}v) = \int_v^1 dt \; f\left(\frac{y_{max}v}{t}, \gamma\right) \frac{y_{max}v}{t^2} \; \mathcal{F}^n(t) \; , \tag{12}$$

in which case the kernel is a sum of terms $K(v,t) = (y_{max}v/t^2) \; f(y_{max}v/t, \gamma)$. The diagonal $K(v,v) \propto f(y_{max})$ corresponds to the diagonal elements K_{bb} in the discretized equation (11). However, for any value of γ, $f(y_{max})$ is extremely small for strong physical reasons: a single nucleon has a vanishing probability of carrying the entire momentum of the nucleus. Thus the matrix $\mathbf{K}$ has very small values along the diagonal and is very close to singular, so this solution method fails.

A standard approach to solving Volterra equations with a kernel vanishing identically along the diagonal is to either integrate Eq. (12) by parts, or to differentiate with respect to x. The first technique gives an integral equation for the primitive of $\mathcal{F}^n(x)$ with kernel $\partial K(x,t)/\partial t$, while the second has kernel $\partial K(x,t)/\partial x$ and left-hand-side $d\widetilde{\mathcal{F}}^n(x)/dx$. These approaches are still problematic, however, because derivatives of the smearing functions are still very small at $y = y_{max}$; also, taking derivatives of functions derived from fits to data introduces substantial errors. Furthermore, the solution depends on knowing $\widetilde{\mathcal{F}}^n(x)$ at *all* values of x, while in practice, only data up to $x = 1$ are available. It is clear that a direct solution to Eq. (9) is impractical for the particular forms of smearing functions used in this model.

B. Multiplicative solution

The most widely-used method for extracting spin-averaged structure functions is the smearing-factor or *multiplicative method* [8]. This is an iterative solution method based on the *ansatz* that the right-hand-side of Eq. (9) can be written as a product of the neutron structure function and a "smearing factor" $S^n(x)$,

$$\widetilde{\mathcal{F}}^n(x) \; = \; S^n(x) \; \mathcal{F}^n(x) \; . \tag{13}$$

From a first guess $\mathcal{F}^{n(0)}(x)$, one obtains $S^{(0)}(x)$ by smearing $\mathcal{F}^{n(0)}(x)$ and dividing by $\mathcal{F}^{n(0)}(x)$. Dividing $\widetilde{\mathcal{F}}^n(x)$ by $S^{n(0)}$ gives $\mathcal{F}^{n(1)}(x)$, so the result after one iteration is

$$\mathcal{F}^{n(1)}(x) \;=\; \widetilde{\mathcal{F}}^n(x)\frac{\mathcal{F}^{n(0)}(x)}{(f \otimes \mathcal{F}^{n(0)})\,(x)} \; . \tag{14}$$

One can see from the form of Eq. (14) that this method is problematic if the smeared structure function has zeros in the range of x of interest. The spin-averaged nuclear structure functions are positive-definite for $0 < x < 1$, so this problem does not arise, and the multiplicative method converges quite rapidly for essentially any reasonable choice of $\mathcal{F}^{n(0)}(x)$. Even for spin-dependent structure functions, which may have several zeros, the multiplicative method works fine as long as the zeros of the smeared $\mathcal{F}^{n(0)}(x)$ are very close to the zeros of $\widetilde{\mathcal{F}}^n(x)$. Since the smearing functions are close to δ-functions, this amounts to requiring that the zeros of the neutron structure function be very close to the zeros of the nuclear structure function. Experimental errors could easily obscure the true location of the zeros of the nuclear structure function, though, making a direct application of this method to experimental data difficult.

C.   Additive extraction method

Instead of assuming a multiplicative smearing factor, one can exploit the fact that the smearing function f is sharply peaked about $y = 1$ to formally write

$$f(y, \gamma) \;=\; \mathcal{N}\ \delta(y - 1) \;+\; \delta f(y, \gamma) \;, \tag{15}$$

where $\mathcal{N} = \int_0^{M_A/M} dy\ f(y, \gamma)$ is the normalization of the smearing function, which for $\gamma = 1$ is either unity for the unpolarized F_2 structure function, or equal to the effective nucleon polarization in the nucleus for the spin-dependent g_1 structure function. The correction δf gives the finite width of the smearing function. The smeared neutron structure function in Eq. (9) can then be written

$$\widetilde{\mathcal{F}}^n(x) \;=\; \mathcal{N}\ \mathcal{F}^n(x) \;+\; (\delta f \otimes \mathcal{F}^n)\,(x) \;. \tag{16}$$

The convolution term in Eq. (16) can thus be treated as a perturbation and the equation solved iteratively. Starting from a first guess $\mathcal{F}^{n(0)}(x)$ one has, after one iteration,

$$\mathcal{F}^{n(1)}(x) \;=\; \mathcal{F}^{n(0)}(x) \;+\; \frac{1}{\mathcal{N}}\left[\widetilde{\mathcal{F}}^n(x) - \left(f \otimes \mathcal{F}^{n(0)}\right)(x)\right] \;. \tag{17}$$

Here, there is no danger of divergences due to zeros in the input, as the only division is by $\mathcal{N}$, which is nonzero for all smearing functions $f(y, \gamma)$.

When $\mathcal{F} = x g_1$, Eq. (9) is a system of two equations, whose solution is slightly more involved. One notes that the function f_{11} is the most sharply peaked of the smearing functions [18], and hence gives the largest contribution to $x g_1^d$. Assuming that the f_{12} contribution is zero, one can apply Eq. (17) to $x g_1^d$ to obtain $g_1^{n(1)}(x)$, which is substituted into the expression for $x g_2^d$. Subtracting this contribution $f_{21} \otimes x g_1^{n(1)}$ from $x g_2^d$ and applying Eq. (17) to the resulting expression then gives $g_2^{n(1)}(x)$. The new value $g_2^{n(1)}(x)$ is then inserted into the $x g_1^d$ equation and the recursive procedure repeated until convergence is achieved.

D. Analysis of convergence

As we will show in Sec. IV below, the convergence of the additive method is quite fast and nearly independent of the initial guess. The reason for this is essentially the sharply peaked shape of the smearing function. This can be illustrated by examining the propagation of the error on the true function $\mathcal{F}_{\text{true}}(x)$ with each iteration i. Starting from a first guess, $\mathcal{F}^{(0)}(x)$, for the true function, we define $\mathcal{F}^{(0)}(x) = \mathcal{F}_{\text{true}}(x) + \epsilon^{(0)}(x)$, where $\epsilon^{(0)}(x)$ is the difference between the first guess and the true result. Tracking this error after $i = 1$ iteration gives

$$\epsilon^{(1)}(x) = \epsilon^{(0)}(x) - \frac{1}{\mathcal{N}} \left(f \otimes \epsilon^{(0)} \right)(x) \ . \tag{18}$$

Note that if $f(y) \sim \delta(y - 1)$, the error for $x < 1$ vanishes even after one iteration. In fact, since $f(y)$ is sharply peaked at $y = 1$ (for the unpolarized and diagonal polarized distributions), $\epsilon^{(1)}(x)$ is expected to be quite small for $x \lesssim 0.8$, regardless of $\mathcal{F}^{(0)}$.

More specifically, the iteration procedure will converge if for successive iterations $|\epsilon^{(i+1)}(x)| < |\epsilon^{(i)}(x)|$. Defining σ to be the width over which the smearing function $f(y) \gg 0$, from Eq.(4) it follows that $\sigma \sim \gamma p_{\text{char}}/M \ll 1$, where p_{char} is the characteristic nucleon momentum scale in the deuteron. Then using the generalized mean value theorem for integrals, the correction term in Eq. (18) can be written as

$$\frac{1}{\mathcal{N}} \left(f \otimes \epsilon \right)(x) \ = \ \epsilon(x/y_*) \ , \tag{19}$$

where $y_* = 1 + c$ is a point within the integration interval, with $|c| < \sigma/2$. If $\epsilon(x)$ is a sufficiently smooth function of x, one can expand the right-hand-side of Eq. (19) in a series

in c,

$$\epsilon(x/(1+c)) = \epsilon(x) - cx\ \epsilon'(x) + \mathcal{O}(c^2) , \qquad (20)$$

so that the error after one iteration is $\epsilon^{(1)}(x) \approx cx\epsilon^{(0)'}(x)$. This then leads to the estimate

$$\left| \frac{\epsilon^{(1)}}{\epsilon^{(0)}} \right| \approx cx \left| \frac{\epsilon^{(0)'}}{\epsilon^{(0)}} \right| < \frac{\sigma}{2} \left| \frac{\epsilon^{(0)'}}{\epsilon^{(0)}} \right| . \qquad (21)$$

so that the ratio of errors $\epsilon^{(1)}/\epsilon^{(0)}$ is proportional to the width of the smearing function, as long as the width is small. Furthermore, because the $i = 1$ error is given by the derivative of $\epsilon^{(0)}$, convergence is fastest when the error is smoothest, which will typically be away from resonance peaks.

IV.   RESULTS

In this section we present numerical results which illustrate the features of the extraction methods discussed in Sec. III. We discuss firstly the unpolarized F_2^n structure function, before considering the more challenging case of the polarized g_1^n structure function.

A.   Unpolarized structure functions

Most previous extractions of the F_2^n structure function have been performed in the deep inelastic region, where the structure functions are smooth and monotonic (beyond $x \sim 0.3$). Before applying our extraction procedure to the more challenging resonance region, we first test the method on the more familiar case of DIS kinematics. For the input proton and neutron structure functions we use the MRST parameterization [25] at $Q^2 = 10$ GeV^2, and simulate the deuteron F_2^d "data" using the finite-Q^2 smearing function $f_0(y, \gamma)$ from Ref. [16].

The resulting extracted neutron F_2^n structure function is shown in Fig. 2 using the additive method. Starting from an initial guess of $F_2^{n(0)} = 0$, the extracted curve is almost indistinguishable from the input F_2^n after just a single iteration. The main reason for this fast convergence is the fact that the nucleons in the deuteron are weakly bound and have small average momentum, which leads to a smearing function $f_0(y, \gamma)$ that is sharply peaked around $y = 1$. Although the precise height and width of the peak may vary slightly for differ-
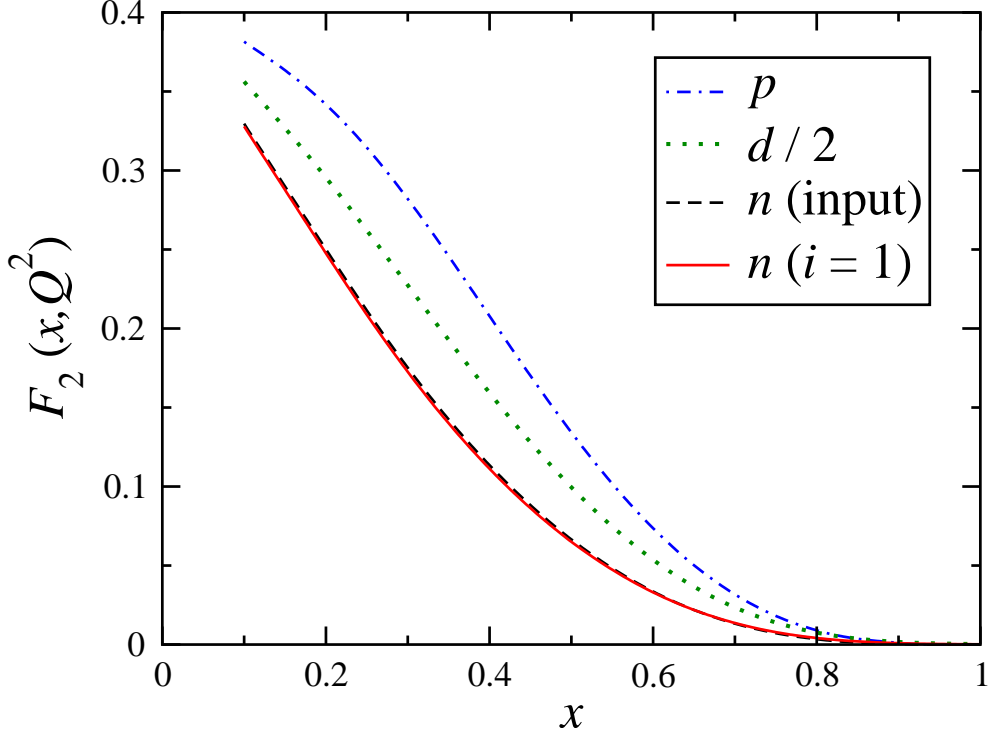
FIG. 2: (Color online) Extraction of the neutron F_2^n structure function at $Q^2 = 10$ GeV^2 from F_2^p (dashed) and F_2^d (dot-dashed) data simulated from the MRST parameterization [25] and the smearing function $f_0(\gamma, y)$ [16] using the additive method. The extracted F_2^n structure function after $i = 1$ iteration (solid) is almost indistinguishable from the input (dotted).

ent deuteron wave functions, the rapid convergence is a relatively model-independent feature of the extraction.

While the extraction of F_2^n in the deep inelastic region is straightforward, obtaining F_2^n in the nucleon resonance region, where the cross section is dominated by resonance peaks, is more problematic. In fact, to our knowledge such an extraction has not yet been undertaken in any quantitative analysis. Even in a system as dilute as the deuteron, the structure of nucleon resonances is significantly smeared out by the Fermi motion of the nucleons, so that for $Q^2 \sim 1$ GeV^2 or higher essentially only the Δ region exhibits any clear resonance structure. In heavier nuclei there is very little resonance structure evident at all [27]. It is not clear *a priori* therefore to what extent neutron resonance data can be extracted from data in which the neutron information is strongly smeared.

To test the effectiveness of the additive extraction method in the resonance region we use as input structure functions from the MAID Unitary Isobar Model [26], which is constructed
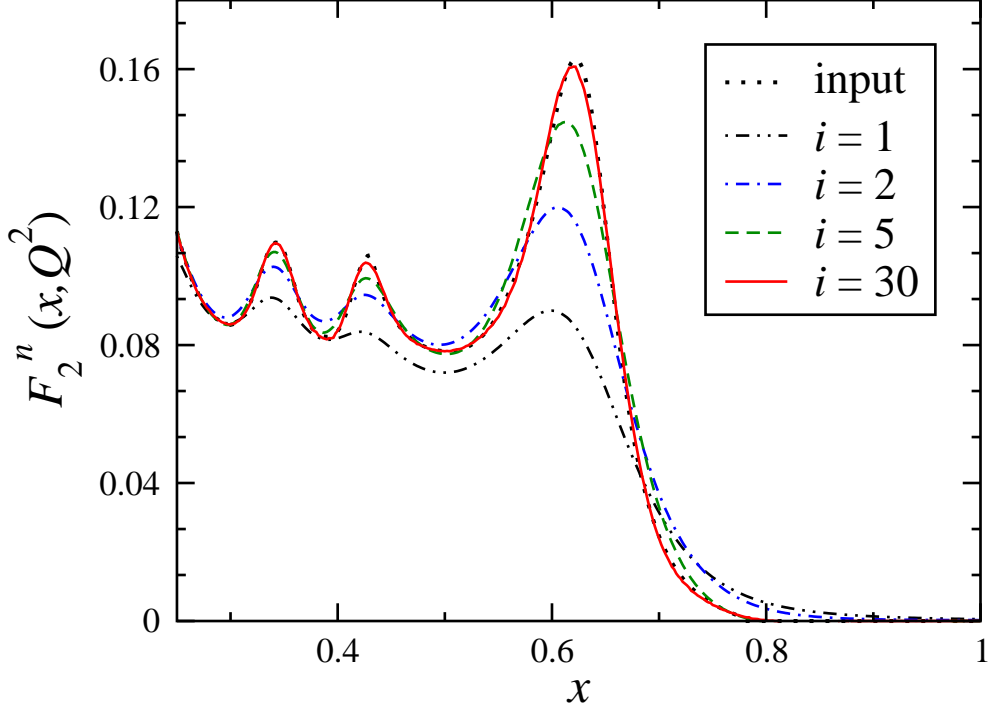
FIG. 3: (Color online) Extraction of the neutron F_2^n structure function at $Q^2 = 1$ GeV^2 in the resonance region using the MAID parameterization [26] for the input (dotted), and a first guess $F_2^{n(0)} = 0$. The convergence of the procedure is illustrated by the results for $i = 1$ (dot-dot-dashed), 2 (dot-dashed), 5 (dashed) and 30 (solid) iterations.

to parameterize meson electroproduction data at low W. The convergence of the iteration procedure in the resonance region is illustrated in Fig. 3, where we attempt to extract the input F_2^n at $Q^2 = 1$ GeV^2 with an increasing number of iterations. Taking as a first guess $F_2^{n(0)} = 0$, after $i = 1$ or 2 iterations the prominent resonant structures are clearly visible, although the amplitudes of the resonance peaks is still underestimated. After $i = 5$ iterations the extracted function is very close to the true result, and would in most cases lie within experimental uncertainties. Repeating the procedure $i = 30$ times reproduces the complete resonance structures almost exactly.

The multiplicative method can also be used to extract F_2^n in the resonance region, as illustrated in Fig. 4. The starting point for the iteration here is taken to be $F_2^{n(0)} = F_2^p$, and after $i = 5$ iterations the result is in good agreement with the input function, only slightly underestimating the peaks of the resonances. As in the additive method, almost perfect agreement can be achieved eventually with further iterations. Note that a direct
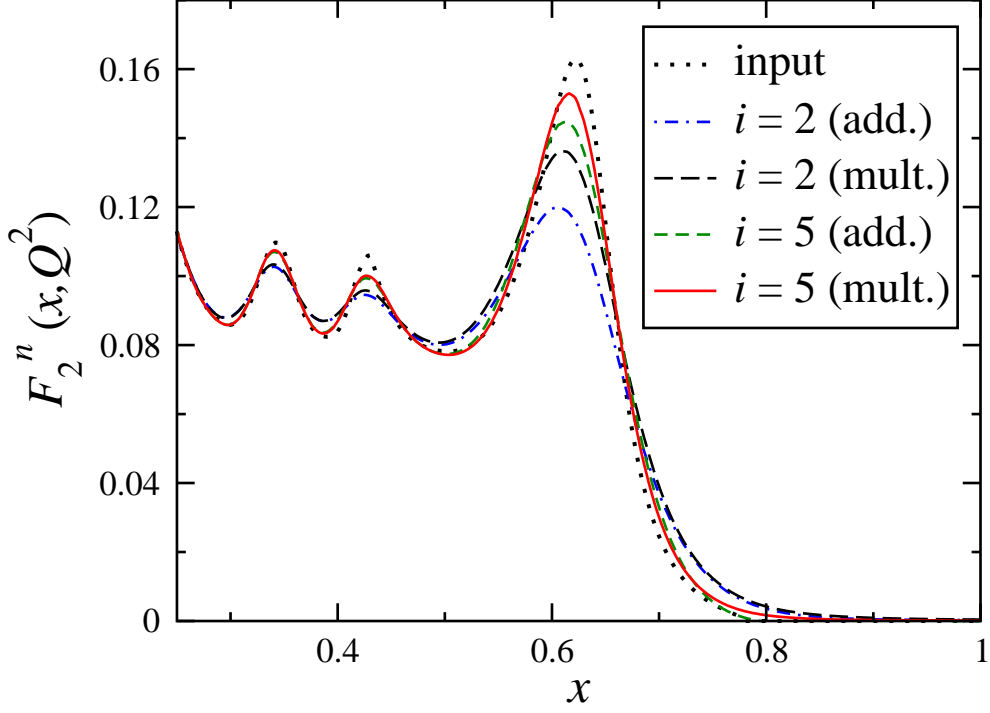
14

FIG. 4: (Color online) Comparison of the convergence of the additive and multiplicative methods for extraction F_2^n for $i = 2$ and 5 iterations. The starting point for the additive method was $F_2^{n(0)} = 0$, while for the multiplicative method $F_2^{n(0)} = F_2^p$. The input structure functions were taken from the MAID parameterization [26] at $Q^2 = 1$ GeV^2.

comparison of the convergence of the additive and multiplicative methods from Fig. 4 is not possible since the starting points $F_2^{n(0)}$ are different. Here we merely illustrate the fact that both methods can converge to the true result within a relatively small number of iterations.

To examine the sensitivity of the extraction to the initial guess $F_2^{n(0)}$, in Fig. 5 we show the result after $i = 2$ iterations for initial guesses $F_2^{n(0)} = 0$ and $F_2^{n(0)} = F_2^p$, using the MAID fit [26] at $Q^2 = 1$ GeV^2 as input. Since the amplitudes of the resonances are significantly larger for the proton than for the neutron, the F_2^p initial guess results in larger amplitudes for the extracted neutron F_2^n for the same number of iterations. On the other hand, because the proton and neutron resonance transitions to the Δ are expected to be equal (since the transitions are isovector), the proton initial guess enables the Δ peak to be reproduced extremely well, in contrast to the zero first guess which requires more iterations to produce the observed structure. Of course, with sufficiently many iterations the input F_2^n can be reproduced accurately regardless of the initial guess $F_2^{n(0)}$.
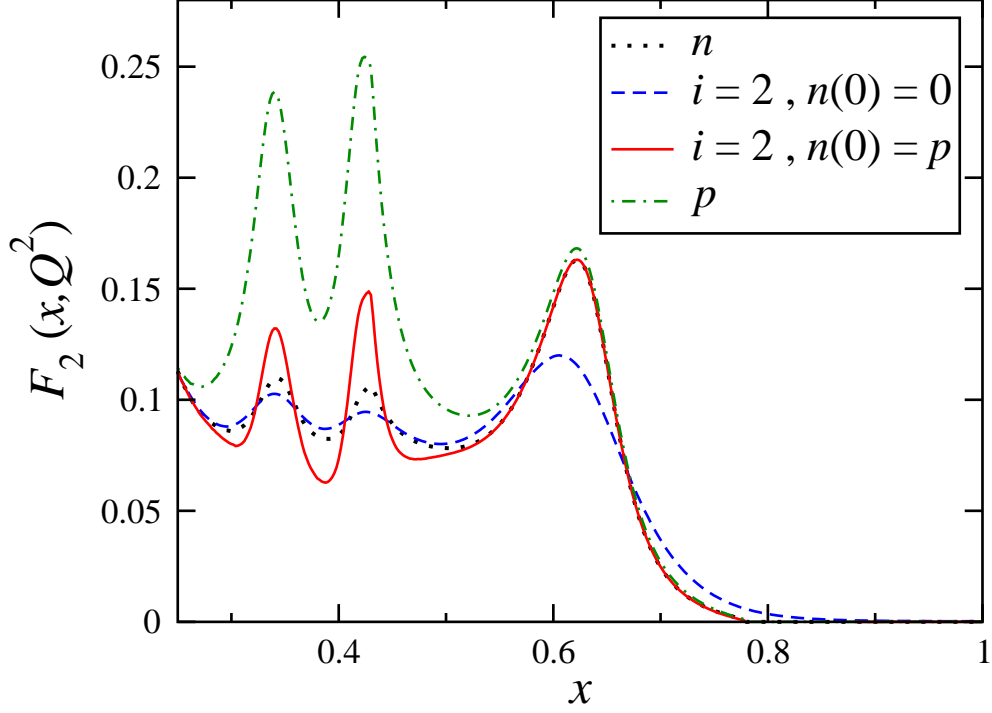
FIG. 5: (Color online) Extracted neutron F_2^n structure function using the additive method with $i = 2$ iterations, starting with initial guesses $F_2^{n(0)} = 0$ (labeled "$n(0) = 0$", dashed) and $F_2^{n(0)} = F_2^p$ (labeled "$n(0) = p$", solid). The input neutron (dotted) and proton (dot-dashed) structure functions are taken from the MAID parameterization [26] at $Q^2 = 1$ GeV^2.

In all of the above extractions the full γ- (or Q^2-) dependent nucleon smearing function $f_0(y, \gamma)$ has been used when computing the deuteron structure function. While using a γ-independent smearing function may be a reasonable approximation in the deep inelastic region where γ values are typically close to unity, applying the $\gamma = 1$ smearing function to low-Q^2, large-x data can lead to errors in the extracted F_2^n, especially in the resonance region [28].

The importance of using the correct smearing function is illustrated in Fig. 6, where we show the extracted neutron F_2^n structure function after $i = 10$ iterations. The result using the full, γ-dependent smearing function is very close to the input. On the other hand, with the Q^2-independent, $\gamma = 1$ smearing function the iteration does not converge to the correct solution. In particular, while a resonance bump is visible in the Δ region, it has the incorrect strength; the second resonance region displays a trough where there should be a peak; and the third resonance region appears to have no structure at all. Increasing the
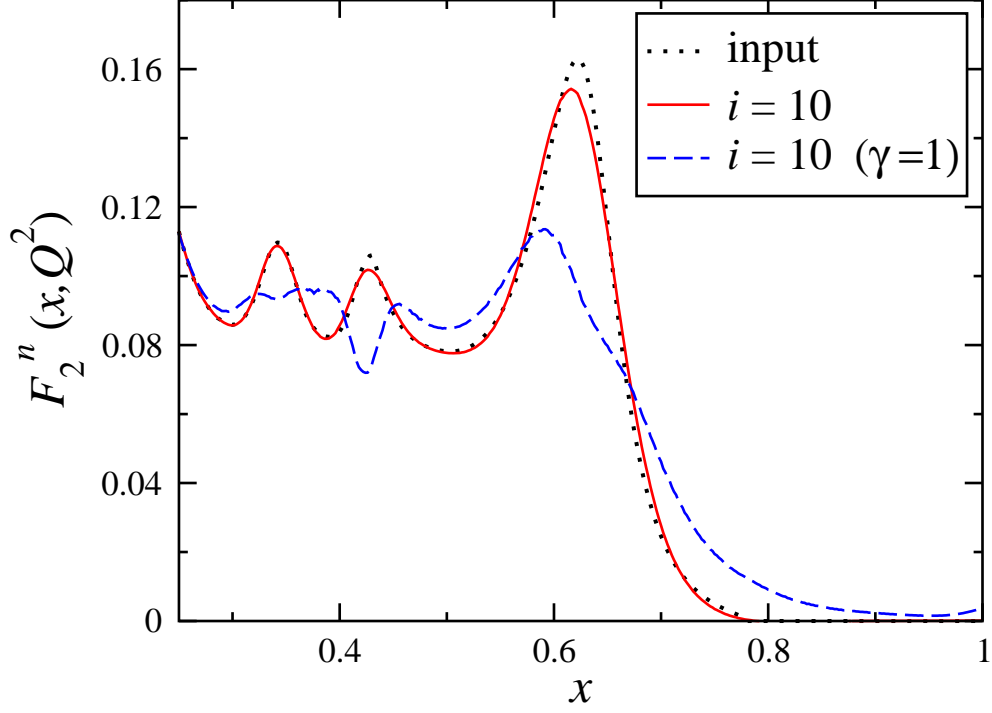
FIG. 6: (Color online) Extracted neutron F_2^n structure function using the additive method after $i = 10$ iterations with the full γ-dependent smearing function (solid) and with the $\gamma = 1$ approximation (dashed), compared with the input neutron (dotted) structure function from the MAID parameterization [26] at $Q^2 = 1$ GeV^2.

number of iterations for the γ-dependent smearing function leads to ever closer convergence to the input F_2^n. For the $\gamma = 1$ smearing function, the result does not change qualitatively with further iterations, however significant noise develops over much of the x range.

These features arise from the mismatch between the smearing functions used to compute the deuteron F_2^d and those used to perform the extraction. Of course, had the deuteron structure function been simulated with the $\gamma = 1$ smearing function, the extraction with the same function would return the same input F_2^n as in Fig. 6. However, this comparison demonstrates the sensitivity of the extraction to the Q^2 dependence of the smearing function, and highlights the importance of using a smearing function with the correct Q^2 dependence when analyzing actual data [29].
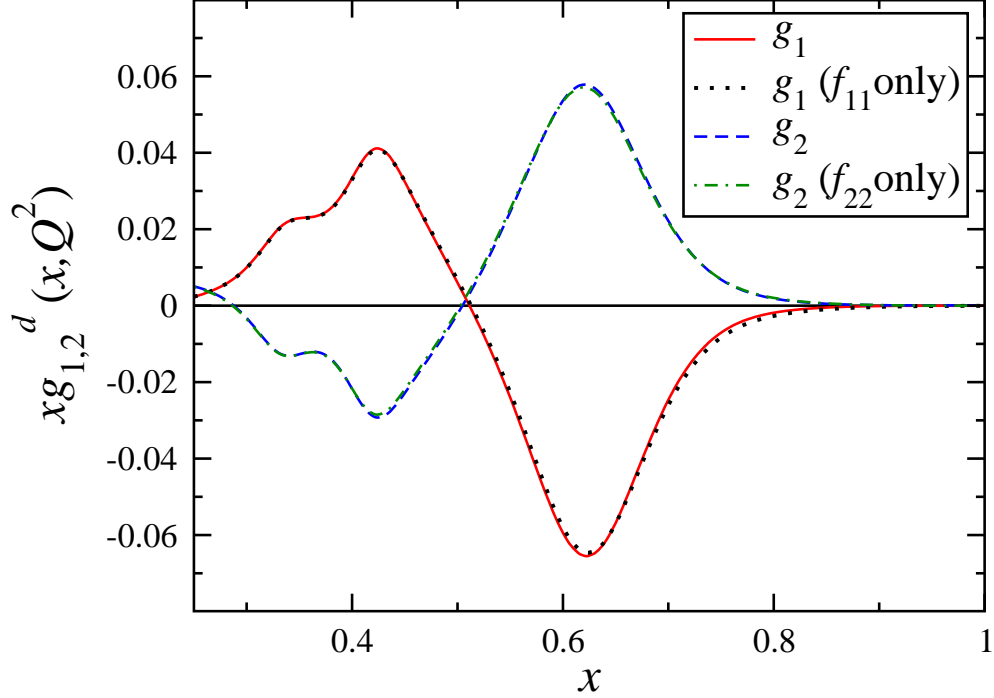
FIG. 7: (Color online) Deuteron xg_1^d and xg_2^d structure functions simulated from the MAID parameterization of the proton and neutron $g_{1,2}$ at $Q^2 = 1$ GeV^2 and the smearing functions f_{ij}, $i, j = 1, 2$, from Ref. [18]. The full results for xg_1^d (solid) and xg_2^d (dashed) are compared with the diagonal approximations using f_{11} only (dotted) and f_{22} only (dot-dashed), respectively.

B. Polarized structure functions

At finite Q^2 the complete expressions for the g_1^d and g_2^d nuclear structure functions in Eq. (3) represent a coupled set of equations involving contributions from both the g_1^N and g_2^N structure functions of the nucleon [18]. While the diagonal f_{11} and f_{22} smearing functions dominate for most kinematics, the off-diagonal f_{12} and f_{21} contributions could be important at low values of Q^2. Furthermore, the g_1^N contribution to g_2^d survives even in the Bjorken limit.

As described in Sec. III C above, one can solve such a system of equations by simultaneously iterating both g_1^n and g_2^n, given known (or simulated) proton and deuteron data. Such a procedure will necessarily be slower and require more iterations, but is stable and will in principle converge to the correct solutions.

In practice, however, for the kinematics discussed here, namely $Q^2 \sim 1$–10 GeV^2, the off-diagonal contributions are rather small. This can be seen in Fig. 7 where we show the xg_1^d

and xg_2^d structure functions simulated from the MAID $g_{1,2}^{p,n}$ parameterizations [26] at $Q^2 = 1$ GeV^2, using the smearing functions $f_{ij}(y, \gamma)$, $i, j = 1, 2$, from Ref. [18]. The results with the diagonal terms only (f_{11} for g_1^d and f_{22} for g_2^d), are very close to the full results which include both diagonal and off-diagonal contributions. With the precision achievable in current and near-term future experiments, the diagonal approximation to the $g_{1,2}^d$ structure functions should therefore provide a reliable framework in which to extract neutron structure functions, and in the following analysis we consider only the diagonal contributions. Furthermore, since the shape of g_2 is qualitatively similar to that of g_1 (generally g_2 has the opposite sign compared with g_1), we shall focus on the g_1 structure function as representative of the effects of extracting spin-dependent neutron structure functions in the resonance region.

As we saw in the previous section, both the additive and multiplicative methods yield reliable results for extracted neutron structure functions, in both the deep inelastic and resonance regions, as long as the structure functions are free of zeros. For polarized scattering the g_1 and g_2 structure functions are no longer positive-definite, so that taking ratios of smeared to unsmeared functions can in principle lead to singularities during the extraction.

This does not necessarily render the multiplicative method completely impractical for extracting polarized structure functions, however. Numerically, for a given iteration where the structure function is close to (but not exactly at) its zero, the smearing factor S^n will be very large. For the next step in the iteration this large contribution will be damped by the corresponding small value of the structure function, making the result finite. On the other hand, precisely how (and whether) this cancellation occurs in practice will be determined by the shapes of the input structure functions and smearing functions, and *a priori* it is not clear whether an extracted non-positive definite structure function will be well-behaved for a particular extraction.

To illustrate the extraction of spin-dependent structure functions we first consider the g_1 structure function in the DIS region in Fig. 8. The input proton xg_1^p and neutron xg_1^n data are taken from the leading twist parameterization in Ref. [30] at $Q^2 = 10$ GeV^2, with the deuteron xg_1^d simulated using the smearing function $f_{11}(y, \gamma)$ from Ref. [18]. With a starting point of $xg_1^{n(0)} = 0$, the extracted neutron structure function after a single iteration using the additive method is essentially indistinguishable from the input. As for the unpolarized F_2 structure function in the DIS region in Fig. 2, this feature reflects the narrow width of the smearing function $f_{11}(y, \gamma)$ around $y = 1$.
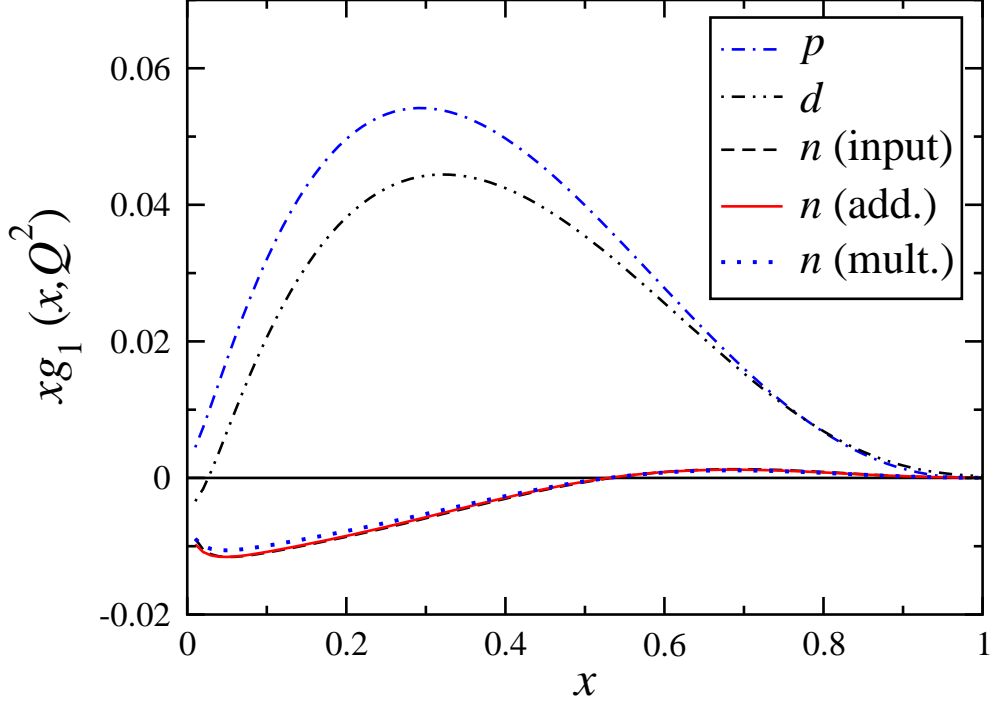
FIG. 8: (Color online) Extraction of the neutron xg_1^n structure function from proton xg_1^p (dot-dashed) and deuteron xg_1^d (dot-dot-dashed) "data" simulated from the leading twist parameterization [30] at $Q^2 = 10$ GeV^2 and the smearing function $f_{11}(\gamma, y)$ [16]. The input (dotted) and extracted xg_1^n functions, for both the additive (solid) and multiplicative (dashed) methods, are almost indistinguishable.

For the multiplicative method the initial guess is taken to be $xg_1^{n(0)} = xg_1^p$, and after one iteration the extracted neutron structure function is also very close to the input. In particular, even though the ratio of smeared to unsmeared g_1^n structure functions is singular at $x \approx 0.5$, the extracted function is nevertheless continuous in this region. The marginally slower convergence here compared with the additive case reflects the different starting inputs for g_1^n, which for the multiplicative method is further from the true result than for the additive.

While both the additive and multiplicative methods appear to be effective in extracting the spin-dependent neutron structure function in the DIS region, their utility in the nucleon resonance region, where the xg_1 exhibits considerably more structure, is compared in Fig. 9 using the MAID parameterization [26] at $Q^2 = 1$ GeV^2. The most striking feature of the extracted neutron xg_1^n is the discontinuities near the zeros of the input function for the
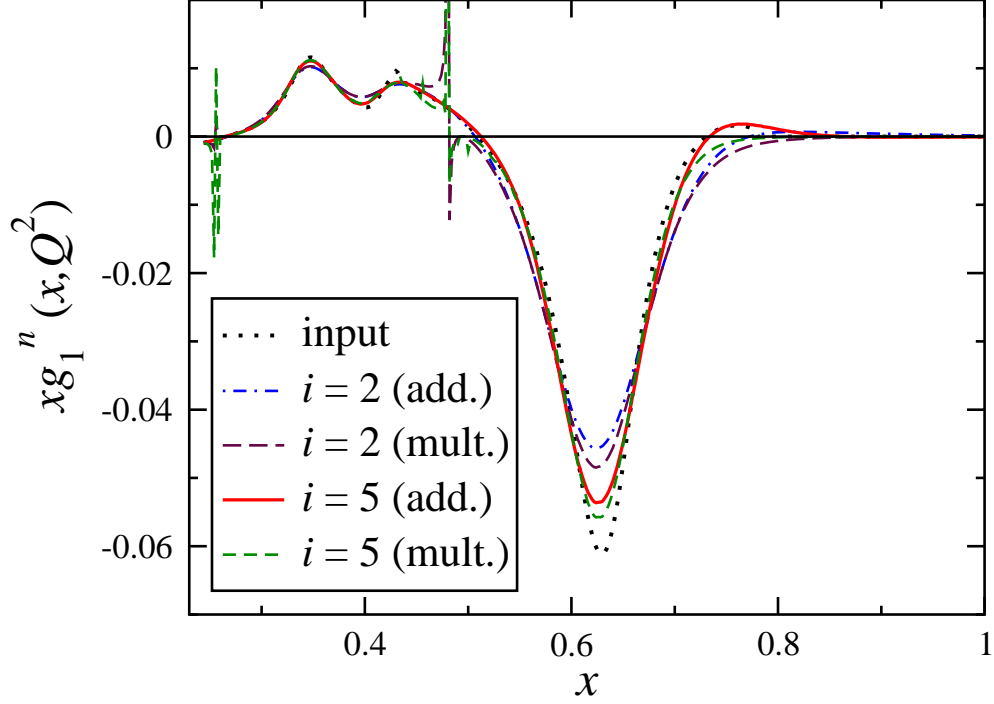
FIG. 9: (Color online) Comparison of the convergence of the additive and multiplicative methods for extraction xg_1^n for $i = 2$ and 5 iterations. The starting point for the additive method was $xg_1^{n(0)} = 0$, while for the multiplicative method $xg_1^{n(0)} = xg_1^p$. The input structure functions were taken from the MAID fit [26] at $Q^2 = 1$ GeV^2.

multiplicative method, which arise from the singularities in the smearing factor S^n. On the other hand, no such singularities appear for the additive method and the extracted functions are smooth and continuous over the entire range of x.

The convergence of the extraction for the additive method is illustrated in Fig. 10, where after only five iterations the extracted xg_1^n displays all of the prominent features of the Δ peak and the higher resonance regions. After $i = 30$ iterations the input function is reproduced almost exactly.

The sensitivity of the extraction to the initial guess for xg_1^n is illustrated in Fig. 11, where the results after $i = 2$ iterations are compared for starting values $xg_1^{n(0)} = 0$ and $xg_1^{n(0)} = xg_1^p$. As in the case of the unpolarized F_2 structure function, the xg_1^p initial guess gives amplitudes that are larger than for the zero initial guess after the same number of iterations. Since the input proton and neutron structure functions are similar in the Δ region, the iteration of xg_1^n converges on the Δ peak more rapidly for the xg_1^p starting point than for the zero first guess.
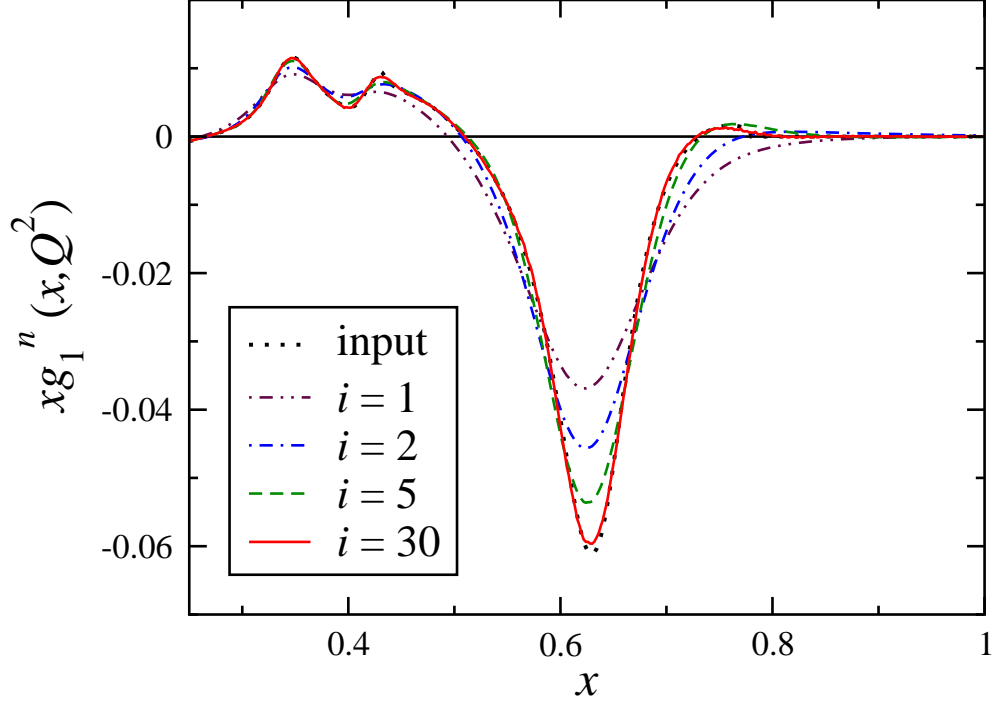
FIG. 10: (Color online) Convergence of the extracted neutron xg_1^n structure function for $i = 1$ (dot-dot-dashed), 2 (dot-dashed), 5 (dashed) and 30 (solid) iterations, using the MAID resonance fit [26] at $Q^2 = 1$ GeV^2 as input (dotted), with a first guess $xg_1^{n(0)} = 0$.

On the other hand, because the second resonance peak for the proton is significantly larger than for the neutron, convergence on this is faster for the $xg_1^{n(0)} = 0$ starting value. Again, with sufficiently many iterations the input xg_1^n can be accurately reproduced independently of the starting point.

The importance of using the correct Q^2 dependence in the smearing function $f_{11}(y, \gamma)$ is highlighted in Fig. 12, where the extracted xg_1^n neutron structure function is shown after $i = 10$ iterations. While the full, γ-dependent smearing function yields an almost exact reconstruction of the input structure function, the result using the $\gamma = 1$ smearing function bears little resemblance to the true xg_1^n. Most notably, the height of the Δ peak is significantly underestimated, and the position of the second resonance peak does not correspond to the correct value. As for the F_2^n structure function in Fig. 6, these features arise from the mismatch between the smearing functions used to compute the deuteron xg_1^d and those used to perform the extraction of xg_1^n. They clearly demonstrate that it is vital to use the correct Q^2 dependence in the smearing function when analyzing data in the nucleon resonance
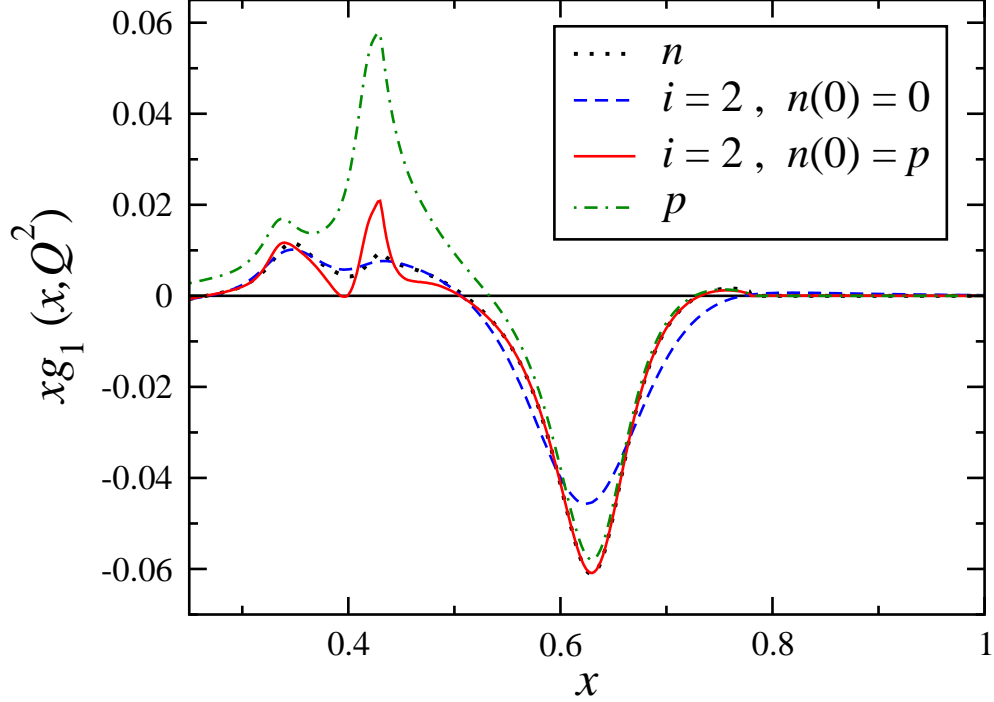
FIG. 11: (Color online) Extracted neutron xg_1^n structure function using the additive method with $i = 2$ iterations, starting with initial guesses $xg_1^{n(0)} = 0$ (labeled "$n(0) = 0$", dashed) and $xg_1^{n(0)} = xg_1^p$ (labeled "$n(0) = p$", solid). The input neutron (dotted) and proton (dot-dashed) structure functions are taken from the MAID fit [26] at $Q^2 = 1$ GeV^2.

region, especially at low Q^2 and large x [31].

Analysis of actual g_1^d (and F_2^d) data to extract the free neutron structure functions will be discussed in a forthcoming publication [29]. However, one can anticipate how the neutron xg_1^n structure function can be extracted from actual proton and deuteron data, together with error bars, by a simple illustration.

In Fig. 13 we show the proton and deuteron structure functions simulated from the leading twist parameterization [30] at $Q^2 = 10$ GeV^2, with the error bars derived from the uncertainties on the xg_1^p and xg_1^n structure functions given in Ref. [30]. The deuteron structure function was simulated by varying each point of the proton and neutron input by a Gaussian of width given by the error bar, which were then smeared with the momentum distribution f_{11} and added to get a "trial" xg_1^d. This procedure was repeated for 50 trials, after which the average and standard deviation of each point was taken to obtain the xg_1^d curves and error bars.
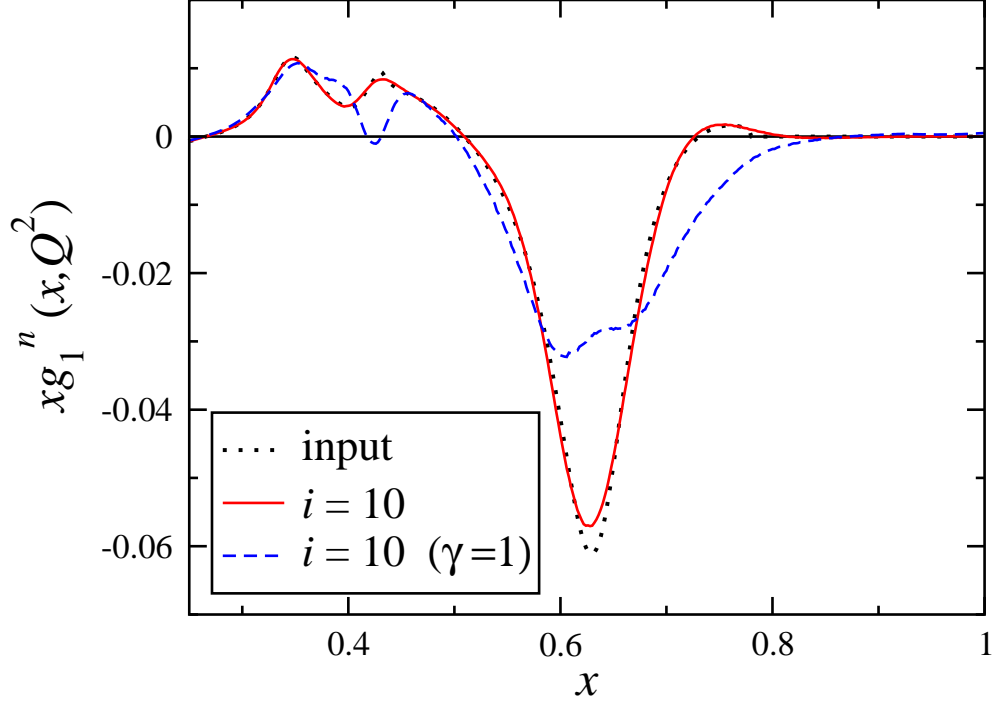
FIG. 12: (Color online) Extracted neutron xg_1^n structure function using the additive method after $i = 10$ iterations with the full γ-dependent smearing function (solid) and with the $\gamma = 1$ approximation (dashed), compared with the input neutron (dotted) structure function from the MAID parameterization [26] at $Q^2 = 1$ GeV^2.

To extract xg_1^n, one can assume that the only errors that contribute are those from the deuteron. In practice, errors on xg_1^d are much larger than those on xg_1^p, and smearing xg_1^p renders the proton errors negligible compared to the deuteron errors. As before, each point of xg_1^d was varied by the error bars, from which the smeared xg_1^p was then subtracted with no errors, and the extraction performed to obtain a "trial" xg_1^n. This was repeated for 50 trials and the average and standard deviation computed as before.

The extracted neutron data points in Fig. 13 are found to be in excellent agreement with the input xg_1^n structure function. The errors on the extracted neutron function after one iteration are of the same order of magnitude as those on the deuteron. Note that the extracted error bars are considerably smaller than the original error bars, indicated by the shaded band around the input xg_1^n, which is mostly due to the fact that, as a sum of smeared functions, the simulated xg_1^d has artificially small errors. For real data, errors on the deuteron and proton structure functions are given, and neglecting the errors on xg_1^p with
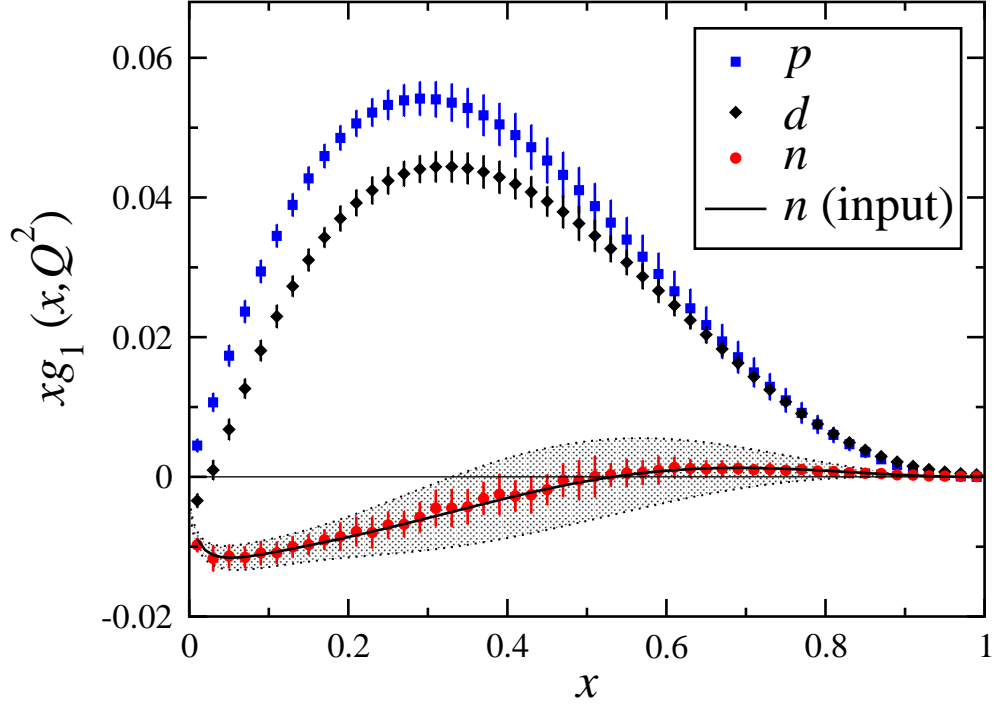
FIG. 13: (Color online) Extraction of the neutron xg_1^n structure function (circles) from proton xg_1^p (squares) and deuteron xg_1^d (diamonds) "data" simulated from the leading twist parameterization [30] at $Q^2 = 10$ GeV^2 and the smearing function $f_{11}(\gamma, y)$ [16]. The error bars are derived from the uncertainties on the structure functions given in Ref. [30]. The input xg_1^n structure function (solid) is given as reference, with uncertainties indicated by the shaded band.

respect to xg_1^d is a very reasonable assumption.

V. CONCLUSIONS

In this paper, we have presented a new method which allows the reliable extraction of neutron structure functions, both spin-averaged and spin-dependent, over a wide range of Q^2. We have compared the new (additive) method to the existing (multiplicative) extraction method, and found that the performance of both methods is very similar for the extraction of F_2^n, while the additive method is free of the singularities that develop when attempting to extract xg_1^n using the multiplicative method. Moreover, the speed of convergence of the additive method is nearly independent of the initial guess, and in most cases a reliable extraction is achieved after $i = 5$ iterations. Finally, the extraction of xg_1^n including error bars, shown in Fig. 13, illustrates both that errors on the extracted function can be reliably

estimated, and that the performance of the method is not overly sensitive to perturbations in the input.

The tests of the additive method on models of resonance-region structure functions show that the general shape of the curve is reproduced after only one iteration, but that further iterations are necessary to accurately extract the magnitude of the resonance peaks. The dependence of the method on the initial guess is evident in the sense that the regions where convergence is slowest are the regions where the initial guess is farthest from the actual magnitude of the resonance peaks. Thus, one can reduce the number of iterations needed with an educated guess about the shape of the neutron function. For example, since the isovector transition to the Δ gives identical proton and neutron structure functions for the resonant part of the Δ, a good first guess for the neutron would always be the proton structure function in the Δ region. To ensure that the extracted neutron structure function is in fact correct in the context of the smearing-function model, one can smear the extracted structure function and add to the smeared proton structure function to compare with the deuteron data.

Despite extensive experiments on light nuclear targets, the neutron remains something of a mystery. The same observables which can be directly measured for the proton must be inferred for the neutron, because its instability outside of the nucleus makes neutron targets impossible. Previously, the low statistics and large errors from experiments designed to measure neutron observables limited the accuracy of measured neutron structure functions far more than using a simplified model of the nucleus to perform the extraction. The situation has changed with recent experiments at JLab, and now accounting for nuclear corrections in neutron structure function extraction procedures is essential to obtain an accurate representation of the neutron structure functions, especially in the resonance region. In particular, we have shown that ignoring finite-Q^2 corrections to nuclear structure functions leads to an extracted neutron structure function which may bear little resemblance to the true shape. To assess quark-hadron duality for the neutron to the same extent that it has been verified for the proton, detailed knowledge of all neutron structure functions in all kinematic regimes is needed. The method presented in this paper, when applied to the most recent JLab data, will be a first step in that direction.

[1] E. D. Bloom and F. J. Gilman, Phys. Rev. Lett. **25**, 1140 (1970).

[2] W. Melnitchouk, R. Ent and C. Keppel, Phys. Rept. **406**, 127 (2005)

[3] F. E. Close and N. Isgur, Phys. Lett. B **509**, 81 (2001); F. E. Close and W. Melnitchouk, Phys. Rev. C **68**, 035210 (2003); S. J. Brodsky, arXiv:hep-ph/0006310.

[4] P. E. Bosted *et al.*, Phys. Rev. C **75**, 035203 (2007); N. Bianchi, A. Fantoni and S. Liuti, Phys. Rev. D **69**, 014505 (2004); A. Airapetian *et al.*, Phys. Rev. Lett. **90**, 092002 (2003); S. Liuti, R. Ent, C. E. Keppel and I. Niculescu, Phys. Rev. Lett. **89**, 162001 (2002); I. Niculescu *et al.*, Phys. Rev. Lett. **85**, 1182, 1186 (2000); G. Ricco, M. Anghinolfi, M. Ripani, S. Simula and M. Taiuti, Phys. Rev. C **57**, 356 (1998).

[5] A. Psaker, W. Melnitchouk, M. E. Christy and C. Keppel, Phys. Rev. C **78**, 025206 (2008).

[6] M. Osipenko, W. Melnitchouk, S. Simula, S. Kulagin and G. Ricco, Nucl. Phys. A **766**, 142 (2006).

[7] P. Solvignon *et al.* [Jefferson Lab E01-012 Collaboration], arXiv:0803.3845 [nucl-ex].

[8] A. Bodek *et al.*, Phys. Rev. D **20**, 1471 (1979); A. Bodek and J. L. Ritchie, Phys. Rev. D **23**, 1070 (1981).

[9] L. W. Whitlow, E. M. Riordan, S. Dasu, S. Rock and A. Bodek, Phys. Lett. B **282**, 475 (1992).

[10] A. Y. Umnikov, F. C. Khanna and L. P. Kaptari, Z. Phys. A **348**, 211 (1994).

[11] C. Ciofi degli Atti, L. P. Kaptari, S. Scopetta and A. Y. Umnikov, Phys. Lett. B **376**, 309 (1996).

[12] W. Melnitchouk, A. W. Schreiber and A. W. Thomas, Phys. Rev. D **49**, 1183 (1994); Phys. Lett. B **335**, 11 (1994); W. Melnitchouk and A. W. Thomas, Phys. Lett. B **377**, 11 (1996).

[13] S. A. Kulagin, G. Piller and W. Weise, Phys. Rev. C **50**, 1154 (1994).

[14] W. Melnitchouk, G. Piller and A. W. Thomas, Phys. Lett. B **346**, 165 (1995); G. Piller, W. Melnitchouk and A. W. Thomas, Phys. Rev. C **54**, 894 (1996).

[15] S. A. Kulagin, W. Melnitchouk, G. Piller and W. Weise, Phys. Rev. C **52**, 932 (1995).

[16] S. A. Kulagin and R. Petti, Nucl. Phys. A **765**, 126 (2006).

[17] S. I. Alekhin, S. A. Kulagin and S. Liuti, Phys. Rev. D **69**, 114009 (2004).

[18] S. A. Kulagin and W. Melnitchouk, Phys. Rev. C **77**, 015210 (2008).

[19] S. A. Kulagin and W. Melnitchouk, Phys. Rev. C **78**, 065203 (2008).

[20] M. Lacombe *et al.*, Phys. Rev. C **21**, 861 (1980).

[21] L. P. Kaptari, A. I. Titov, E. L. Bratkovskaya and A. Y. Umnikov, Nucl. Phys. A **512**, 684 (1990); W. Melnitchouk and A. W. Thomas, Phys. Rev. D **47**, 3783 (1993).

[22] J. Golak *et al.*, Phys. Rept. **415**, 89 (2005).

[23] Y. Horikawa, F. Lenz and N. C. Mukhopadhyay, Phys. Rev. C **22**, 1680 (1980).

[24] P. Linz, *Analytical and Numerical Methods for Volterra Equations*, Philadelphia: SIAM, 1985.

[25] A. D. Martin, R. G. Roberts, W. J. Stirling and R. S. Thorne, Eur. Phys. J. C **28**, 455 (2003).

[26] D. Drechsel, O. Hanstein, S. S. Kamalov and L. Tiator, Nucl. Phys. A **645**, 145 (1999).

[27] J. Arrington, R. Ent, C. E. Keppel, J. Mammei and I. Niculescu, Phys. Rev. C **73**, 035205 (2006).

[28] P. E. Bosted and M. E. Christy, Phys. Rev. C **77**, 065206 (2008).

[29] Y. Kahn *et al.*, in preparation.

[30] J. Blümlein and H. Böttcher, Nucl. Phys. B **636**, 225 (2002).

[31] K. V. Dharmawardane *et al.*, Phys. Lett. B **641**, 11 (2006); Jefferson Lab Experiment E93-009, G. Dodge, S. Kuhn and M. Taiuti spokespersons, and S. Kuhn and N. Guler, private communication; Jefferson Lab Experiment E01-006, O. Rondon-Aramayo spokesperson.